

1 Transformed-Stationary EVA 2.0: A 2 Generalized Framework for Non-Stationary 3 Joint Extremes Analysis

4 Mohammad Hadi Bahmanpour¹, Alois Tilloy², Michalis Vousdoukas³, Ivan Federico⁴, Giovanni
5 Coppini⁴, Luc Feyen², Lorenzo Mentaschi^{1,4}

6
7 ¹ Department of Physics and Astronomy “Augusto Righi” (DIFA), University of Bologna, Bologna,
8 Italy

9 ² European Commission, Joint Research Centre, Ispra, Italy

10 ³ Department of Marine Sciences, University of Aegean, University Hill, Mytilene, Greece

11 ⁴ CMCC Foundation - Euro-Mediterranean Center on Climate Change, Italy

12
13 Corresponding author:

14 Mohammad Hadi Bahmanpour

15 University of Bologna

16 Email: hadi.bahmanpour@unibo.it

17 Abstract

18 The increasing availability of extensive time series on natural hazards underscores the need for robust
19 non-stationary methods to analyze evolving extremes. Moreover, growing evidence suggests that
20 jointly analyzing phenomena traditionally treated as independent, such as storm surge and river
21 discharge, is crucial for accurate hazard assessment. While univariate non-stationary extreme value
22 analysis (EVA) has seen substantial development in recent decades, a comprehensive methodology for
23 addressing non-stationarity in joint extremes—compound events involving simultaneous extremes in
24 multiple variables—is still lacking. To fill this gap, here we propose a general framework for the non-
25 stationary analysis of joint extremes that combines the Transformed-Stationary Extreme Value
26 Analysis (tsEVA) approach with Copula theory. This methodology implements sampling techniques to
27 extract joint extremes, applies tsEVA to estimate non-stationary marginal distributions using GEV or
28 GPD distributions, and utilizes time-dependent copulas to model evolving inter-variable dependencies.
29 The approach’s versatility is demonstrated through case studies analyzing historical time series of
30 significant wave height, river discharge, temperature, and drought, uncovering dynamic dependency
31 patterns over time. To support broader adoption, we provide an open-source MATLAB toolbox that
32 implements the methodology, complete with examples, available on GitHub.

1. Introduction

Extreme value analysis (EVA), or frequency analysis of extreme events, is crucial for understanding the likelihood of catastrophic events. By quantifying the probabilities of such occurrences, EVA informs design approaches and supports the development of better management strategies. Traditionally, EVA assumes stationarity, meaning that the statistical properties of the data, such as mean and variance, remain constant over time (Coles, 2001). However, many long-term datasets reveal varying degrees of non-stationarity, often due to anthropogenic influences and natural climate variability. Ignoring non-stationarity can lead to inaccurate estimates of probabilities and return levels, underscoring the importance of accounting for time-dependent changes in the frequency and intensity of extreme events (Cheng, et al., 2014).

In a univariate framework, non-stationarity refers to temporal changes in the frequency or magnitude of a single random variable. Univariate non-stationary EVA is a relatively well-explored topic (e.g., Cannon, 2010; Parey, et al., 2010). A common approach to address non-stationarity involves defining a parametric form for its variation, potentially as a function of covariates, and using optimization methods, such as the Maximum Likelihood Estimator (MLE), to determine the optimal parameters that capture both the non-stationary behavior and the distribution of extreme values. Other methods focus on stationarizing the input series and performing EVA on this stationarized data (Parey et al., 2010; Parey et al., 2013; Mentaschi et al., 2016; Acero et al., 2017; Parey et al., 2019). Mentaschi et al. (2016) proposed an alternative approach to univariate non-stationary EVA that decouples the detection of non-stationarity from the fit of the Extreme Value Distribution (EVD). Known as transformed-stationary EVA (tsEVA), this method transforms a non-stationary signal into a stationary one, avoiding the need for predefined parametric forms for non-stationarity. Unlike traditional methods, which parameterize time-dependent changes and optimize them alongside the EVD parameters, tsEVA focuses on ensuring that the transformed signal adheres to the principles of asymptotic extreme value theory. While mathematically equivalent to traditional approaches, tsEVA offers key advantages: (a) it does not rely on assuming specific parametric forms for non-stationarity and (b) it provides intermediate diagnostics to verify the effectiveness of the transformation. This well-established methodology has been widely adopted in various studies for univariate non-stationary EVA (e.g., Mentaschi et al., 2017; Dosio et al., 2018; Naumann et al. 2021; Vousdoukas et al., 2018; Dottori et al., 2023).

From a risk assessment perspective, studies (e.g. Zscheischler et al. 2018, 2020) have highlighted that univariate approaches can misrepresent the probability of joint extreme events, particularly in risk management and infrastructure design. Multivariate extreme value analysis (EVA) provides a more robust framework for accurately quantifying risk in such contexts (Tilloy, et al., 2020). Its applications span a wide range of hazards, including drought-heatwave events (e.g. Manning et al. 2019), compound hydrological events (e.g. Bevaqua et al. 2017; Jiang et al. 2022), and coastal hazard (e.g. Bevaqua et al. 2019).

Similar to the univariate case, multivariate extreme value analysis (EVA) for datasets with long temporal coverage must account for the non-stationarity of the underlying signals. Several studies have investigated non-stationary joint distributions, though these efforts often focus on specific applications rather than development of general methodologies. For example, Bender et al. (2014) applied a non-stationary statistical model to analyze the time-varying joint distribution of flood peak and volume for the Rhine River. Wahl et al. (2015) analyzed the joint occurrence of storm surge and precipitation for major US coastal cities and demonstrated that compound flooding events have increased significantly over the past century, with higher risk along the Atlantic and Gulf coasts. Jiang et al. (2015) examined how reservoir construction influenced joint return periods of low river flow downstream, incorporating

80 non-stationarity in both marginal distributions and dependence structures using temporal variation and
81 covariates. Similarly, Sarhadi et al. (2016) assessed non-stationary drought characteristics, including
82 severity and duration, by combining historical and projected Standardized Precipitation Index (SPI)
83 data under various climate scenarios. Li et al. (2019) studied spatial variations in extreme precipitation,
84 modeling non-stationarity in margins and dependencies through a linear regression applied to a 30-year
85 moving time window.
86 Despite these efforts, such applications are often tailored to specific problems and lack generalizability.
87 While univariate non-stationary EVA is relatively well-studied, multivariate non-stationary EVA
88 remains an underexplored field with no widely accepted standard approach. To address this gap, here
89 we extended the tsEVA methodology to develop a versatile method for the multivariate analysis of
90 non-stationary extremes, grounded in copula theory (Sklar, 1959, 1973). This enhanced framework
91 provides a generalizable solution for capturing the dependence structures and time-varying
92 characteristics of extreme events across multiple variables. The capabilities of the resulting open-
93 source MATLAB toolbox, tsEVA 2.0, are demonstrated in this study through a series of applications
94 that showcase its utility in different scenarios. These examples highlight the potential of tsEVA 2.0 to
95 advance the understanding and modeling of multivariate non-stationary extremes in a range of
96 scientific and engineering contexts.

97 2. Data and Methods

98 Non-stationary copula

100 The term 'copula', introduced by Sklar's theorem (1959), refers to a mathematical tool that describes the
101 dependency between different univariate distributions, known as marginals in this context. Given a set
102 of random variables (Y_1, \dots, Y_m) with marginal distributions F_1, \dots, F_m and joint distribution function
103 $H \in \mathcal{H}(y_1, \dots, y_m)$, the copula C is a function defined in the probability space such that:

$$106 H_{Y_1, \dots, Y_m}(y_1, \dots, y_m) = C(F_{Y_1}(y_1), \dots, F_{Y_m}(y_m)) \quad (1)$$

107 Equation (1) illustrates why copulas are widely used in higher-dimensional statistics, as they enable
108 separate modeling of the marginals and their dependency structure, simplifying the construction of joint
109 distributions. For a more detailed description of the copula theory, the reader is referred to Joe (1997)
110 and Nelsen (2006). In this study we considered three well-established types of copulas (Table 1):

- 112 1. **Gaussian copula.** In this copula, the joint probability density function exhibits symmetry around a
113 central point, with the contours of constant density forming ellipsoids in the multivariate space. The
114 Gaussian copula models situations where the dependency structure between two variables remains
115 constant across the entire distribution and does not exhibit tail dependence.
- 116 2. **Gumbel copula.** This is an Archimedean copula, i.e. it models the dependencies among variables using
117 a function of the marginal probability, called "generation function", able to capture non-linear
118 dependencies. In particular, the Gumbel copula can adequately reproduce conditions when the
119 dependency among variables is stronger for the upper tails. For higher-dimensional cases (trivariate and
120 above), we use a C-vine construction, which builds the multivariate dependence from pairwise Gumbel
121 copulas in a hierarchical tree structure.
- 122 3. **Frank copula.** This is an Archimedean copula that suits situations that are tail-independent in both tails,
123 meaning that as values approach extreme highs or lows, the dependence between them weakens.

125 Table 1: list of copula functions implemented in tsEVA 2.0. In the table, the symbol $\phi()$ represents the standard normal distribution. For
 126 Archimedean copulas (e.g., Gumbel and Frank) $\gamma_\theta(\chi)$ denotes the generator function used in constructing the copula
 127 $c(u, v|\theta) = \gamma_\theta^{-1}[\gamma_\theta(u) + \gamma_\theta(v)]$.
 128

Copula	$c(u, v \theta)$	$\gamma_\theta(\chi)$	Parameter range
Gaussian	$\int_{-\infty}^{\phi^{-1}(u)} \int_{-\infty}^{\phi^{-1}(v)} \frac{1}{2\pi\sqrt{1-\theta^2}} \exp\left(\frac{2\theta xy - x^2 - y^2}{2(1-\theta^2)}\right) dx dy$	-	$\theta \in [-1, 1]$
Gumbel	$\exp\left\{-\left[(-\ln u)^\theta + (-\ln v)^\theta\right]^{1/\theta}\right\}$	$(-\ln \chi)^\theta$	$\theta \in [1, \infty)$
Frank	$-\frac{1}{\theta} \ln\left(1 + \frac{(e^{-\theta u} - 1)(e^{-\theta v} - 1)}{e^{-\theta} - 1}\right)$	$-\ln \frac{e^{-\theta \chi} - 1}{e^{-\theta} - 1}$	$\theta \in \mathbb{R} \setminus 0$

129
 130 To describe the time evolution of the copula, we evaluated a time-varying coupling parameter θ_t on a
 131 moving window, similar to what proposed by Li, et al., (2019). The duration of series is covered by N
 132 time windows where:

$$133 \quad N = \left\lfloor \frac{T-w}{\Delta t} \right\rfloor + 1 \quad (2)$$

134 Where T is the length of the series (in years), w is the window length (in years), $\Delta t = 1$ is the window
 135 shift (sliding by 1 year), and N is the number of moving windows. The symbol $\lfloor \cdot \rfloor$ ensures a floor
 136 operation.
 137

138 Non-stationary marginals

139
 140 The treatment of the marginals (i.e., the distributions of the univariates, F_1, \dots, F_m in equation 1), was
 141 performed in accordance with the univariate theory of extremes. There are two popular approaches that
 142 are used to model extremes of a series. The Fisher-Tippett-Gnedenko theorem establishes the
 143 Generalized Extreme Value (GEV) distribution as the appropriate distribution for statistically
 144 homogeneous block maxima, such as annual maxima. The cumulative GEV distribution is defined as:
 145

$$146 \quad GEV_X(x; \varepsilon, \mu, \sigma) = \exp\left\{-\left[1 + \varepsilon \left(\frac{x-\mu}{\sigma}\right)\right]^{-1/\varepsilon}\right\}, \quad (3)$$

147
 148 where ε, μ , and σ are the shape, location and scale parameters, that need to be found out through a
 149 fitting process. On the other hand, the Generalized Pareto Distribution (GPD) is the general form of the
 150 distribution of the Peaks Over Threshold (POT) according to the Pickands–Balkema–De Haan theorem.
 151 The cumulative GPD is defined as
 152

$$153 \quad GPD_{X-u}(\tilde{x}; \varepsilon, \tilde{\sigma}) = 1 - \left(1 + \frac{\varepsilon \tilde{x}}{\tilde{\sigma}}\right)^{-1/\varepsilon}, \quad (4)$$

154
 155 where $\tilde{x} = x - u$ is the series of excess values relative to the selected threshold value (u), and ε and $\tilde{\sigma}$
 156 are the shape and scale parameters respectively (Coles, 2001).

157 To address non-stationarity in the marginal distributions, we adopted the approach proposed by
 158 Mentaschi et al. (2016), which demonstrates that a transformation formally equivalent to local
 159 normalization allows for a generalized representation of non-stationary extreme value distributions
 160 while maintaining a constant shape parameter. Specifically, the transformation f is defined as:
 161

$$162 \quad y(t) \xrightarrow{f(y,t)} x(t) \quad \text{where} \quad f(y, t) = \frac{y(t) - T_y(t)}{c_y(t)} \quad (5)$$

163

164 where $y(t)$ is the non-stationary series, $x(t)$ is the assumed stationary series, $T_y(t)$ and $C_y(t)$ are
 165 generic terms representing the long-term variation in the mean and amplitude of $y(t)$, respectively. A
 166 back-transformation from the stationary domain x to the non-stationary one y leads to a formulation of
 167 parameters of time-varying extreme values distribution. In particular, for the GEV one obtains:

$$168 \begin{cases} \varepsilon_y = \varepsilon_x \\ \sigma_y(t) = C_y(t) \cdot \sigma_x \\ \mu_y(t) = C_y(t) \cdot \mu_x + T_y(t) \end{cases}, \quad (6)$$

169 and for the GPD:
 170
 171

$$172 \begin{cases} \varepsilon_y = \varepsilon_x \\ \tilde{\sigma}_y(t) = C_y(t) \cdot \tilde{\sigma}_x \\ u_y(t) = C_y(t) \cdot u_x + T_y(t) \end{cases}. \quad (7)$$

173
 174

175 Joint sampling of the extremes

176

177 There are several methods to sample joint extremes from multivariate data (e.g., Zheng et al., 2014).
 178 The simplest method used in tsEVA 2.0 applies a block-maxima technique, compatible with GEV-
 179 distributed marginals, focusing on the coupling of annual maxima from each variable. A key limitation
 180 of this method, inherent to the GEV distribution, is that not all extremes are annual maxima, nor are all
 181 annual maxima truly extreme events. Additionally, this approach may link events far apart in time
 182 while missing those that occur close together but fall across block boundaries. Despite these
 183 limitations, its simplicity makes it effective for studying dependencies among relatively slow, seasonal
 184 phenomena, such as drought and heat waves.

185 A more advanced approach involves non-stationary joint Peaks Over Threshold (POT) sampling. This
 186 method first applies the transformation in Eq. 5 to convert each non-stationary signal $y(t)$ to a
 187 stationary series $x(t)$. POT sampling is then conducted on each stationarized series $x(t)$, selecting
 188 multivariate peaks within a defined maximum time interval $\Delta t_{multivariate}$. A challenge with this
 189 approach is the potential for multiple combinations of univariate peaks within the interval
 190 $\Delta t_{multivariate}$. In tsEVA 2.0, this issue is addressed by prioritizing joint peaks with the largest mean
 191 values (average of univariate peak values), iteratively removing all other peak combinations.

192

193 Goodness-of-fit

194

195 To evaluate the goodness-of-fit (GOF) of the copula model, a multi-parameter approach was employed
 196 by analyzing a set of statistics that quantify the similarity between the fitted distribution and the
 197 empirical data. Specifically, the following statistics were considered:

- 198 • Cramér-von Mises statistic. Its general definition is:

$$S_n = \int [C_n(u) - C_\theta(u)]^2 du, \quad (8)$$

199 where C_n is the empirical distribution, C_θ is the theoretical fit, u is defined in the domain of the
 200 distributions. The statistic S_n serves as a proxy for the distance between the empirical and
 201 theoretical distributions in probability space. In this study, we applied the rank-based version of the
 202 Cramér-von Mises statistic, where the ranks of C_n and C_θ are compared using Monte Carlo

simulations. For non-stationary distributions, S_n is estimated separately over different time windows, and the results are averaged, to provide the mean Cramér-von Mises statistic \overline{S}_n .

- For each bivariate sub-distribution, the goodness-of-fit was evaluated by comparing the correlation structure of the fitted copula to that of the original data. Specifically, the differences in Spearman's rank correlation coefficient ($\Delta\rho_{Spearman}$) and Kendall's tau ($\Delta\tau_{Kendall}$) were computed between a Monte Carlo simulation of the fitted copula distribution and the empirical values derived from the original sample. This provides a measure of how well the fitted model captures the dependency structure of the data. For multivariate non-stationary copulas, this analysis was extended by computing the average differences $\Delta\rho_{Spearman}$ and $\Delta\tau_{Kendall}$ over all the bivariate sub-distributions and the considered time windows. The metrics are defined as:

$$\overline{\Delta\rho_{Spearman}} = \frac{1}{N \cdot P} \sum_{t=1}^N \sum_{1 \leq i < j \leq d} |\rho_{t,(i,j)} - \rho_{t,(i,j),MC}| \quad (9)$$

$$\overline{\Delta\tau_{Kendall}} = \frac{1}{N \cdot P} \sum_{t=1}^N \sum_{1 \leq i < j \leq d} |\tau_{t,(i,j)} - \tau_{t,(i,j),MC}| \quad (10)$$

where $\rho_{t,(i,j)}$ and $\rho_{t,(i,j),MC}$ are the Spearman correlation of variables i and j at time window t for the original and Monte-Carlo samples, $P = \frac{d \cdot (d-1)}{2}$ is the total number of bivariate pairs, d is the total number of variables, N is the total number of windows, $\tau_{t,(i,j)}$ and $\tau_{t,(i,j),MC}$ are the Kendall correlation of variables i and j at time window t for the original and Monte-Carlo samples, and $\overline{\Delta\rho_{Spearman}}$ and $\overline{\Delta\tau_{Kendall}}$ are the absolute difference in Spearman and Kendall correlation averaged across time windows and across bivariate pairs of variables.

Bivariate Return Periods

In the non-stationary context, there is not any standard definition of a return period, and different propositions have been made (Yan et al. 2017). Therefore, the interpretation of return periods requires careful definition, and different frameworks have been proposed (Parey et al. 2010; Yan et al. 2017). In Parey et al. (2010), univariate return levels are computed for the stationary transformed variable and then back-transformed to represent a specific target future climate period. The tsEVA framework adopts a similar transformation-based philosophy but with a different implementation and interpretation.

Multivariate return periods can be defined in several ways (Serinaldi, 2015; Salvadori et al., 2016). In tsEVA 2.0, we adopted the following two definitions:

- (1) A definition that is more relevant in risk analysis and represent simultaneous exceedance of variables over their given thresholds (the AND return period) which for bivariate case, reads as:

$$T_{u_1, u_2}^{AND} = \frac{\mu}{1 - u_1 - u_2 + C(u_1, u_2)} \quad (11)$$

- (2) A definition that is closest to the definition of cumulative multivariate distribution function (the OR return period) which for the bivariate case, reads as:

$$T_{u_1, u_2}^{OR} = \frac{\mu}{1 - C(u_1, u_2)} \quad (12)$$

where μ is the average inter-arrival time, representing the mean time between peaks and $u_i = F_{x_i}(x_i)$ represents continuous marginal distributions. The OR return period (T_{u_1, u_2}^{OR}) refers to the case where at least one of the x_i values is exceeded while the AND return period T_{u_1, u_2}^{AND} represent the case where both of the variables have exceeded x_i values. In bivariate analysis, joint probabilities associated with return periods form level curves (also known as isolines). Based on the above definition, we restricted the use of joint return periods to bivariate cases only. In the non-stationary context, return periods are conditional on the statistical properties (marginals and dependence) of each time window. The computation procedure is as follows: For each time window, we estimate (i) the time-varying marginal distributions from the back-transformed non-stationary GEV or GPD parameters, and (ii) the copula function $C(u, v)$ from the coupling parameter specific to that window. These are combined using the AND and OR definitions (Equations 11 and 12) to compute joint exceedance probabilities.

Detection of non-stationarity

The Mann-Kendall (MK) test is a nonparametric method used to detect trends in data over time. It compares pairs of data points to identify a consistent upward or downward trend. After calculating a test statistic, a p-value is obtained and compared to a chosen significance level (α) to determine whether the trend is statistically significant. A p-value below α indicates a significant trend, while a larger p-value suggests the trend is not statistically significant. A commonly used value for α is 0.05, but it can be adjusted depending on the context and requirements of the analysis.

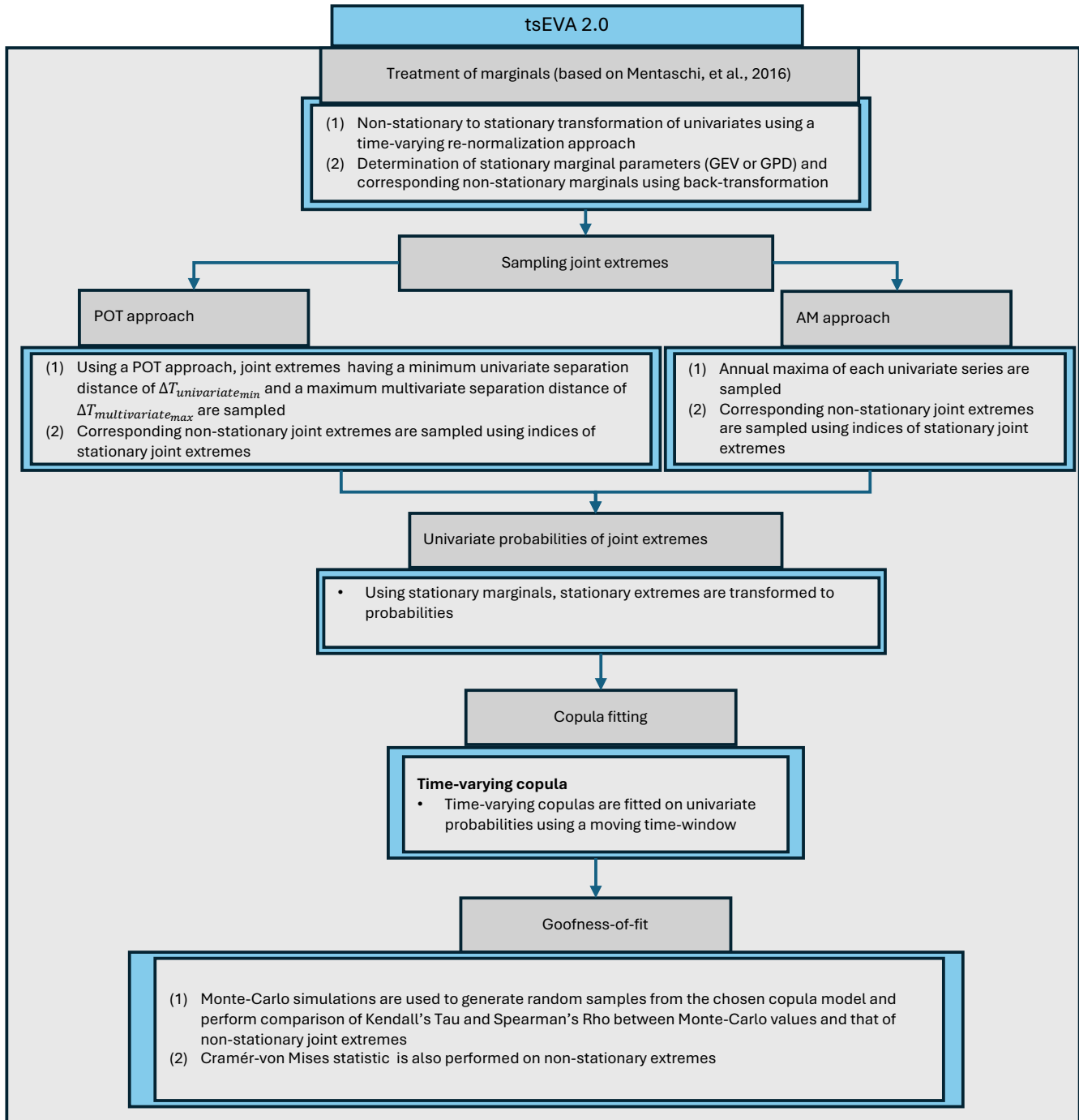
We used MK to assess non-stationarity of the univariate marginals by applying the test on the annual percentile series. To see the effectiveness of transformation, the test was applied on both stationary and non-stationary series (i.e., before and after application of transformation). This method was applied as a shortcut to other sophisticated tests for stationarity that rely on bootstrapping (e.g., Parey, et al., 2013). To assess the non-stationarity of the joint distribution, we applied the modified Mann-Kendall test (Hamed 2008; Hamed and Rao 1998; Yue and Wang 2004), which explicitly accounts for autocorrelation arising from the 1-year sliding window used to compute the temporal evolution of the coupling parameter. By considering this autocorrelation, the test provides a more accurate assessment of statistical significance, avoiding the overestimation of trend significance that can occur with overlapping windows.

Assembling the Pieces: the tsEVA 2.0 toolbox

The methodologies outlined above are integrated into a MATLAB toolbox tsEVA 2.0, an extension of the original tsEVA by Mentaschi, et al., 2016, providing a versatile framework for multivariate analysis of non-stationary extremes across various applications. The toolbox features two primary functions: one employing non-stationary multivariate POT sampling with GPD and the other utilizing multivariate block-maxima sampling with GEV (Figure 1).

In both approaches, the analysis begins by applying tsEVA's method to transform each univariate time series from non-stationary to stationary. The extreme value distribution (either GPD or GEV) is then fitted to the stationary series, and the resulting distributions are back-transformed into the time-varying domain to represent the non-stationary marginals. Joint extremes are subsequently sampled and mapped into probability space using the stationary marginals. A copula is then fitted to this transformed dataset, which can either be stationary (assuming constant dependency over time) or non-stationary

286 (accounting for time-varying dependency). To ensure the appropriateness of each copula model in
 287 representing the joint distribution of non-stationary extremes, we developed a dedicated goodness-of-fit
 288 routine. A flowchart of tsEVA 2.0 is presented in Figure 1.
 289



290
 291 *Figure 1: Flowchart of tsEVA 2.0*

292
 293
 294 Case studies
 295

296 To demonstrate the applications of the general method developed for analyzing non-stationary joint
297 extremes, the methodology was applied to three case studies, each selected to highlight specific
298 features of the new methodology. All the data in the following examples were obtained from model
299 results. Possible biases in the model data can also find its way into quantification of return periods.
300 Nonetheless, these model outputs provided a good basis upon which the general methodology
301 developed in this paper could be substantiated. For the wave dataset used in the first and second case
302 study, we used a bias-corrected version of the results reported in Mentaschi, et al., 2023. The bias
303 correction was based on Quantile mapping, and we focused on values above 50th percentile. The bias-
304 correction was based on comparison with satellite measurements.

305

306 **1. Joint extremes of river discharge and wave height:**

307 This case study explored the evolving relationship between river discharge and significant wave height
308 (SWH) near the coast over time. The focus was on the mouth of the La Liane River in France, a fast-
309 responding river influenced by precipitation. Wave data comprised 3-hourly SWH records from a high-
310 resolution global wave model (Mentaschi et al., 2023) with nearshore resolutions of 2–4 km, covering
311 the period 1950–2020. River discharge data was obtained from the HERA hydrological reanalysis
312 (Tilloy et al. 2025). The dataset, generated with the OS LISFLOOD model (Burek et al. 2013),
313 provides high resolution (approx. 1.5 km) simulation of river discharge for every river with an
314 upstream area $>100\text{km}^2$ across Europe.). The data comes at six-hourly records over the same time
315 frame. Although residual model biases contribute to uncertainty in return level estimation, the use of
316 model data for coastal hazard mapping is widely established practice, as models provide complete
317 spatiotemporal coverage that cannot be achieved through sparse observational networks. The wave
318 dataset employed in this study (Mentaschi et al., 2023) was post-processed to reduce biases through
319 quantile mapping against satellite observations. Likewise, the river discharge dataset (Tilloy et al.
320 2025) was evaluated using 2448 river gauging stations to assess model skill.

321 The analysis used the Generalized Pareto Distribution (GPD) for univariate margins and a time-varying
322 Gumbel copula to model dependence. Univariate peaks were selected with a minimum separation of 30
323 days. In this case study, joint extremes were defined as events in which the peak of river discharge
324 occurred within a maximum time lag of 45 days after the peak of wave height. The choice of a 45-day
325 maximum allowable lag among bivariate peaks reflects the time-lag among univariate peaks (30 days)
326 and the impact-based temporal compounding perspective (Zscheischler et al., 2020): when an extreme
327 sea level event compromises coastal system capacity, a subsequent extreme river discharge within 45
328 days can produce amplified impacts even without direct hydrodynamic interaction. Following
329 sampling, the average temporal separation among bivariate peaks was approximately 15 days. Non-
330 stationarity of the joint distribution was assessed within a 40-year moving window, with thresholds set
331 at the 95th percentile for river discharge and the 99th percentile for wave height. On average, each 40-
332 year window contains 66 joint extremes, which provides adequate sample sizes for stable copula
333 parameter estimation.

334

335 **2. Spatial correlation of extreme wave heights across three locations:**

336 The second case study evaluated the spatial relationship of SWH across three locations scattered
337 around the Marshall Islands, using the same source for wave dataset as the first case study. This
338 trivariate analysis highlighted spatial dependencies, employing a non-stationary Gumbel copula with
339 non-stationary margins, modeled with GPD. Each variable was sampled at the 99th percentile, with
340 univariate peaks spaced a minimum of 12 hours apart and a maximum allowable distance of 12 hours
341 for multivariate peaks. A 40-year time window was used for the joint distribution. Each time window
342 contained 76 joint extremes on average.

343

344 **3. Joint Distribution of Surface Temperature and SPEI:**

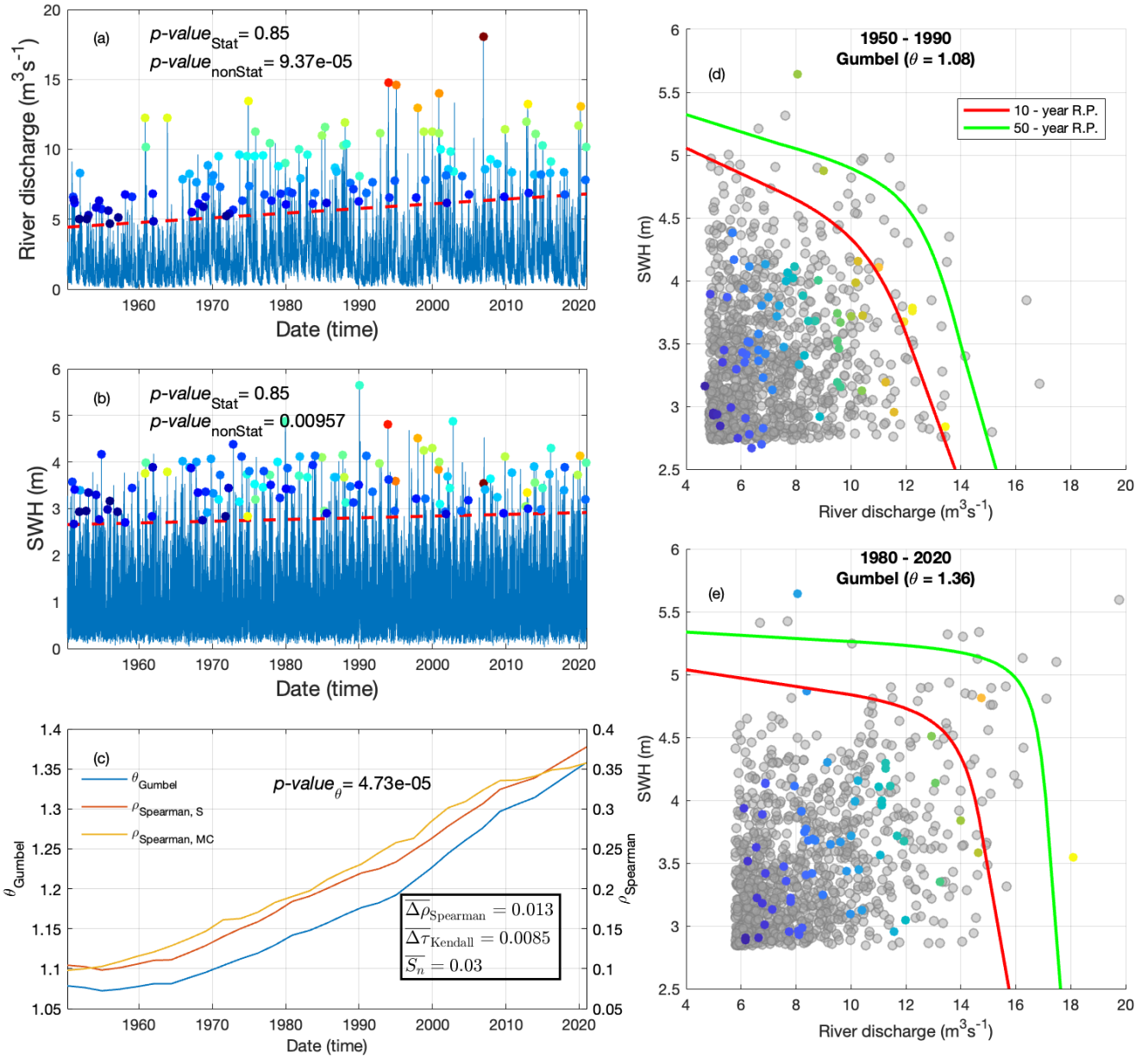
345 The third case study examined the relationship between surface temperature and the 6-month
346 Standardized Precipitation-Evapotranspiration Index (SPEI) in a region south of Milan, Italy (9.25E,
347 45.25N). Hourly surface temperature data from the ECMWF ERA-5 dataset (1959–2023) was paired
348 with monthly SPEI data (1959–2022) (Zhang, 2023). To better capture heatwave dynamics, the
349 temperature data were smoothed using a 10-day running mean. The analysis was restricted to the period
350 from April to September, which aligns with the growing season when drought impacts are at their peak
351 and heatwaves present a significant hazard. This case study demonstrated a scenario where block-
352 maxima sampling is a valid and simpler alternative to the POT method for analyzing extremes. A 35-
353 year non-stationary time window was used in this analysis for the joint distribution.
354
355

356 3. Results

357 3.1. Case study 1: joint extremes of river discharge and wave height

358 The non-stationarity of both time series was assessed using the Mann-Kendall test, which revealed
359 significant increasing trends in both variables (Figure 2a–b). The effectiveness of transformation was
360 verified by p-values both before and after transformation (Figure 2a-b). Among the evaluated copula
361 models, the Gumbel copula was the best fit for representing the dependence structure with this copula's
362 goodness of fit parameters presented in Figure 2c. Applying a time-varying Gumbel copula with a 40-
363 year moving window revealed a statistically significant increasing trend in the dependency parameter,
364 denoted as θ_{Gumbel} (Figure 1c). A similar upward trend was observed in the Spearman correlation
365 coefficient ρ_{Spearman} , calculated for both the sampled joint extremes and Monte Carlo-generated
366 samples.

367 To illustrate these findings, two representative time windows were selected, comparing the theoretical
368 Gumbel copula (gray dots, based on Monte Carlo simulations) with the sampled joint extremes (Figure
369 2d–e). These panels visually confirmed a stronger coupling between the two variables toward the end
370 of the time series. This increase of coupling was also evident in shape of level curves corresponding to
371 10 and 50-year return periods. Furthermore, the analysis of joint return periods revealed substantial
372 shifts in level curves between the beginning and end of the series (curves in Figure 2d–e),
373 demonstrating the utility of this technique in capturing temporal variations (non-stationarity) in joint
374 extremes.
375



376
 377
 378
 379
 380
 381
 382
 383
 384
 385
 386

Figure 2: Analysis of joint extremes of river discharge and wave height off La Liane river mouth. In panels (a)-(b) the input series are presented (blue line). The thick dashed red line is the time-varying threshold level while the colored dots indicate the joint extreme events. The color of dots was based on events having the largest mean value. Also shown in these two plots is the p-value of Mann-Kendall test of the percentile series applied on both stationary (denoted by Stat) and non-stationary (denoted by nonStat) series. Variation with time of the copula parameter was depicted in panel (c) with a p-value of Mann-Kendall test. Other goodness-of-fit parameters of the non-stationary copula model were shown in panel (c). A 10-window smoothing was applied to curves of panel (c) for better representation. The time-varying Spearman correlation coefficient of the samples (red line) and Monte-Carlo values (yellow line) were also presented in panel (c). Panels (d) – (e) present the overlay of joint extremes (colored dots) and Monte-Carlo values (gray dots) in two different time windows (1950 – 1990) of (1980 – 2020) with the copula parameter indicated above. The 10 and 50-year joint return levels (using the AND definition) are also shown in these panels (colored curves).

387 3.2. Case study 2: trivariate joint extremes of significant wave height

388 The co-occurrence of extreme SWH at three locations (P1–P3) around the Marshall Islands was
389 examined as the second case study (Figure 3). Univariate non-stationarity was evaluated using the
390 Mann-Kendall test (Figure 3b, f, i), which revealed the strongest non-stationarity at P2, as indicated by
391 its lowest p-value. Both P1 and P3 also exhibited positive trends, significant at the 90% confidence
392 level. The effectiveness of transformation for each bivariate pair was assessed by comparing p-values
393 before and after transformation (Figure 3b, f, i). The transformation clearly influenced the detected
394 trends with all pairs showing p-values greater than 0.7 after the stationarizing step.

395 Non-stationarity in the coupling was evaluated using a time-varying Gumbel copula model, showing
396 significant increasing trends in correlation for all pairs (p-value < 0.05) (Figure 3e). Notably, the
397 correlations for P1–P3 and P1–P2 have p-values near zero, whereas the correlation for P2–P3 is
398 approximately 0.03 (Figure 3e). The pairs of extremes of SWH exhibited a change in correlation with
399 time, with the Gumbel coupling parameter changing from 1.98 to 2.46 for P1–P2 pair, 2.05 to 2.43 in
400 P1–P3, and 1.42 to 1.61 in P2–P3 (Figure 3c-d, g-h, j-k). The Monte Carlo extractions (gray dots in
401 Figure 3c-d, g-h, j-k) closely matched the data samples, demonstrating good agreement. The goodness-
402 of-fit metrics indicated accurate results, with $\overline{\Delta\rho_{Spearman}} = 0.13$, $\overline{\Delta\tau_{Kendall}} = 0.11$, $\overline{S_n} = 0.07$ (Figure
403 3a).

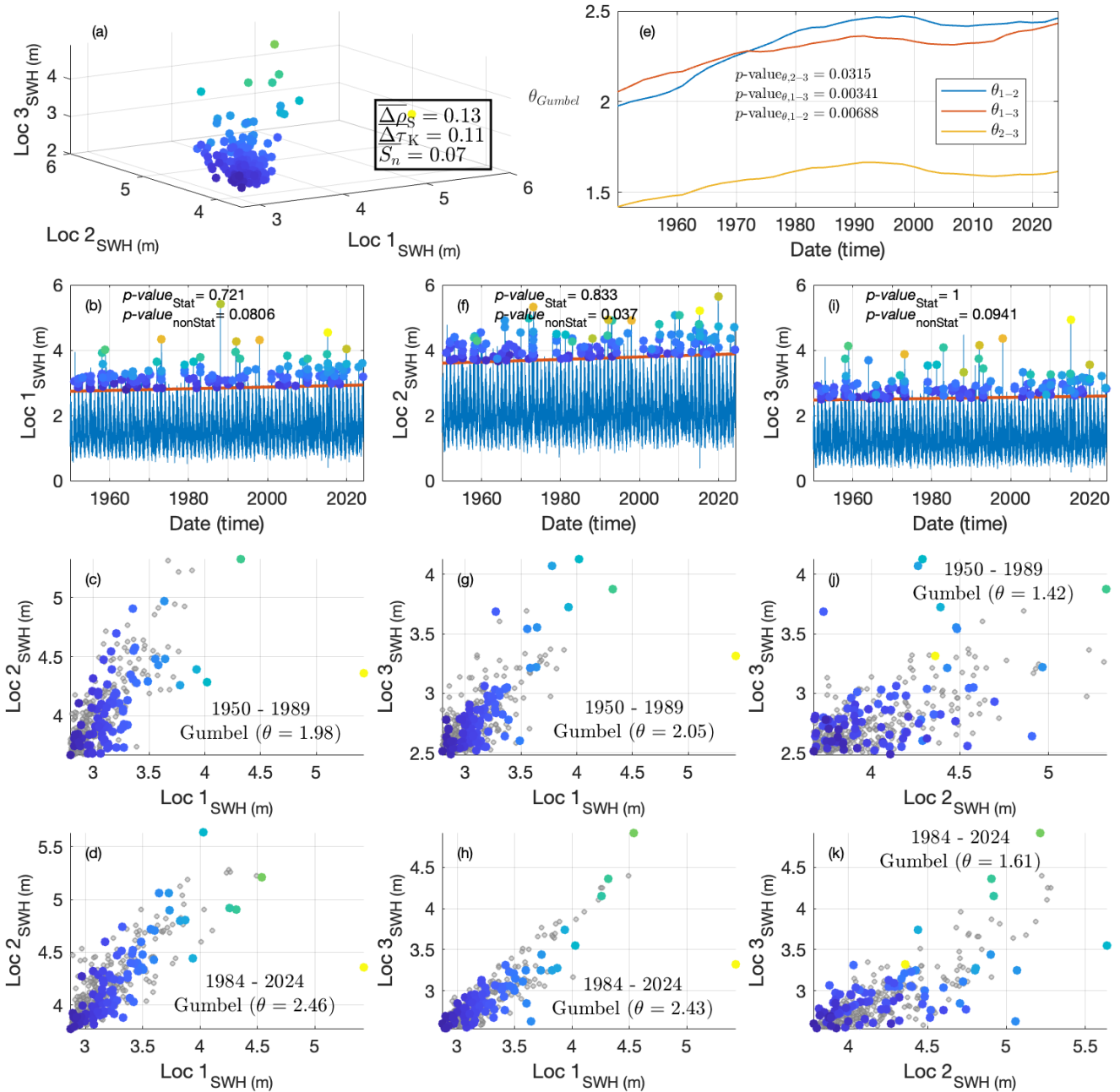
404

405

406

407

408



409
 410 *Figure 3: Analysis of trivariate extremes of SWH in neighboring locations near Marshall Islands. Goodness-of-fit parameters and*
 411 *sampled extremes are presented in panel (a). Univariate extremes (colored dots) and threshold levels (thick red lines) along with the*
 412 *p-value of the Mann-Kendall test of the percentile series applied on both stationary (denoted by Stat) and non-stationary (denoted by*
 413 *nonStat) series are presented in panels (b), (f) and (i). Panels (c), (d), (g), (j), (k) and (i) present overlaying of pairs of extremes (colored*
 414 *dots) and Monte-Carlo values (gray dots) with the copula parameter and time window indicated above each panel. The time-varying*
 415 *coupling parameter of each pair of extremes and the p-value of the Mann-Kendall test of the coupling parameter is presented in panel (e).*
 416 *A 10-window smoothing was applied to curves of panel (e).*

417
 418 3.3. Case study 3: joint extremes of surface temperature and SPEI

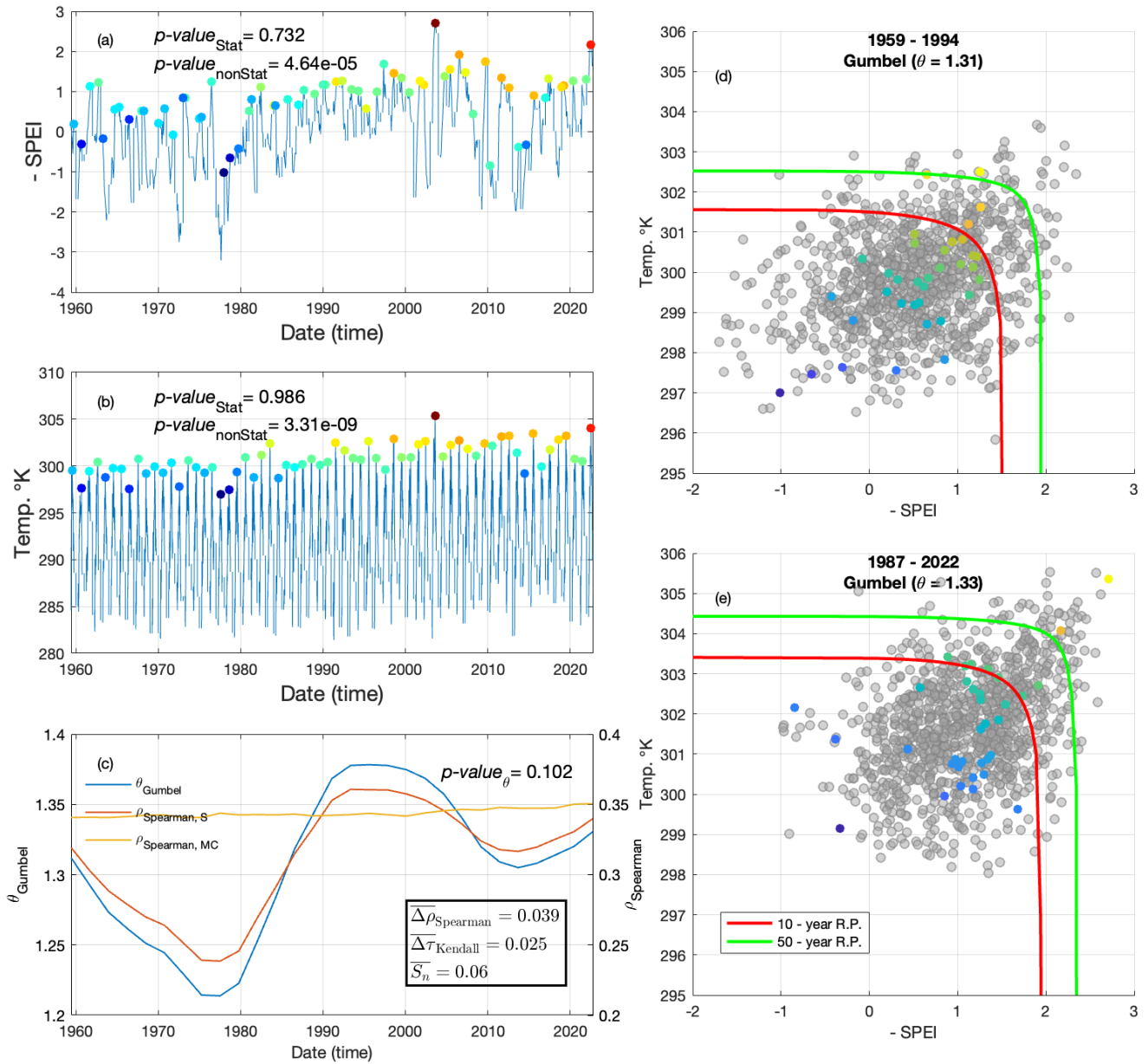
419 The final case study examines joint extremes of surface temperature and the SPEI at an inland location
 420 south of Milan, focusing on the period from April to September. In this case, an annual maxima
 421 sampling technique was employed to identify univariate extremes (Figure 4a–b), and the Gumbel

422 copula was used to model their joint distribution. Consequently, the marginals were estimated using the
423 GEV distribution.

424 Non-stationarity in both series was assessed through the Mann-Kendall test, with p-values close to zero
425 (Figure 4a-b). The p-values increased significantly after the transformation based on comparison of p-
426 values obtained from original non-stationary and transformed stationary series (Figure 4a-b). Based on
427 goodness-of-fit statistics ($\overline{\Delta\rho_{Spearman}}$, $\overline{\Delta\tau_{Kendall}}$ and $\overline{S_n}$), the Gumbel copula was identified as the best-
428 performing model for representing the joint distribution of extremes (Figure 4c). The application of a
429 non-stationary Gumbel copula allowed for the estimation of a time-varying coupling parameter (blue
430 curve in Figure 4c). However, unlike the previous two examples, no significant trend was detected in
431 the time-varying coupling parameter (Figure 4c). This indicates that the non-stationarity in the joint
432 distribution was solely driven by the non-stationarity of the marginals. The Spearman correlation
433 parameter of the joint extremes also indicated lack of significant trend (red line; Figure 4c). Thus, in
434 this example a constant coupling parameter was adopted (mean of the blue curve in Figure 4c).

435 Subsequently, the Monte-Carlo samples generated based on the coupling parameter indicated near-
436 constant Spearman correlation parameter (yellow line; Figure 4c). The evolving interrelationships of
437 extremes was also verified by a visual inspection of different time windows across the duration of
438 series (Figure 4d-e). Evidently, the Gumbel copula was a good representation for co-occurrences of
439 extremes, where stronger dependencies was observed in the upper tail of both time windows (Figure
440 4d-f). The non-stationarity of the marginals resulted in change of level curves corresponding with 10
441 and 50-year joint return periods (colored curves in Figure 4d-f).

442



443
 444 *Figure 4: Analysis of annual extremes of SPEI and temperature (°C). Panels (a)–(b) display the input series (thin blue line) alongside the*
 445 *annual maxima (colored dots), where SPEI values have been multiplied by -1 for interpretability. The color of the dots reflects the mean*
 446 *values of the joint extremes. The p-value from the Mann-Kendall test applied on both stationary (denoted by Stat) and non-stationary*
 447 *(denoted by nonStat) series for the annual maxima is also reported in these panels. Panel (c) presents the goodness-of-fit parameters for*
 448 *the copula model, along with the time-varying coupling parameter (left axis) (thick blue line) and the time-varying Spearman*
 449 *correlation coefficient, calculated for both the original samples and the Monte Carlo values (right axis). A 10-window smoothing was applied to*
 450 *curves of panel (c) for better representation. Panels (d)–(e) overlay the joint extremes (colored dots) with Monte Carlo values (gray dots),*
 451 *simulated based on the constant coupling parameter specified in each panel. The level of agreement between the observed and simulated*
 452 *values demonstrates the validity of the fitted copula model. Also shown in these two panels is the joint return levels (using AND*
 453 *definition) corresponding with the 10 and 50-year return levels (colored curves).*

454 Discussion

455 Extreme Value Analysis (EVA) is a robust and widely used method for estimating the frequency of rare
 456 and impactful events. However, the growing availability of long-term, large-scale time series for

457 hazard-related variables, from both historical and climate studies, has increasingly demonstrated that
458 the assumption of stationarity, a cornerstone of EVA, often does not hold. In the case studies examined
459 in this research, statistically significant trends were observed across all the time series analyzed.
460 Moreover, beyond significant temporal changes in the extremes of many univariate series, clear non-
461 stationarity was also observed in the dependencies between different variables. This study highlights
462 the importance of considering non-stationarity in modeling joint distribution of natural hazard data.
463

464 The first case study explores the relationship between river discharge and coastal hazard-related
465 variables, such as significant wave height (SWH). While the coupling between these variables is
466 relatively weak, it remains statistically significant, indicating that the likelihood of compound events is
467 higher than would be expected if the variables were independent. Among the three tested copula
468 models, the Gumbel copula demonstrated the best fit, capturing the stronger dependency observed in
469 the upper tails. The analysis of the Liane River discharge and the SWH near its mouth over the past 70
470 years reveals a significant upward trend in both variables, as evidenced by p-values approaching zero
471 (Figure 2a-b). Correspondingly, the coupling parameter has shown a marked increase over time, with
472 the Spearman correlation rising from less than 0.1 in 1950 (a low but statistically significant value) to
473 over 0.37 in 2020 (Figure 2c). This growing interdependence has led to a pronounced upward shift in
474 the AND return level curves (Figure 2d-e). This significant growth in coupling may be attributed to two
475 factors: the inherent stronger upper-tail dependency captured by the Gumbel copula and the increasing
476 frequency of extreme values in both river discharge and SWH. These findings suggest that while the
477 underlying dynamics of the coupling have remained stable, the amplification of extremes in both
478 variables have intensified their overall interdependence during joint peak events.
479

480 The second case study investigates the spatial dependency of extremes in a hazard-related variable,
481 specifically significant wave height (SWH). This aspect is critical for risk assessment, as hazards often
482 exhibit strong spatial coherence. When an extreme event, such as a severe storm, impacts one location,
483 it is highly likely to affect neighboring areas as well. Consequently, hazards at different locations
484 cannot be assumed to be statistically independent (e.g., Vousdoukas et al., 2020). Previous studies have
485 examined spatial dependencies of extreme SWH using satellite altimeter observations or sparse buoy
486 data (e.g., Shooter et al., 2021; Jane et al., 2016; Wang et al., 2024). These works aimed to quantify
487 spatial dependence in extreme wave events, offering valuable insights for coastal inundation studies
488 and the creation of hazard maps. In this case study, high-resolution numerical wave model data from
489 Mentaschi et al. (2023) were employed to assess the spatial correlation of extreme SWH, accounting
490 for non-stationarity in the marginal distributions and coupling intensity. The analysis focused on three
491 locations near the Marshall Islands, approximately 250 km apart for P1-P2 and P1-P3, and 350 km
492 apart for P2-P3. These locations are in a region characterized by numerous small islands that act as
493 natural barriers, attenuating wave energy from certain directions. Despite these geographical features,
494 the dependency between the variables remains significant. The degree of coupling in extreme SWH
495 among the three locations shows a clear relationship with their spatial separation. The comparable
496 distances between P1-P2 and P1-P3 correspond to similar levels of dependency in extreme wave
497 events, with correlation values increasing from 1.98 and 2.05 at the start of the time series to 2.46 and
498 2.43 by its end, respectively. In contrast, the greater distance between P2-P3 results in a weaker
499 dependency, with correlations starting at about 1.42 and rising to 1.61 over the same period. The
500 growing dependency among SWH at the three locations is supported by the Mann-Kendall test applied
501 to the coupling parameter. The test results indicate a p-value near zero for the pairs P1-P2 and P1-P3,
502 while the pair P2-P3 has a p-value of approximately 0.03. This observed increase in spatial dependency
503 across all pairs suggests that not only have extreme events intensified in the region, but their spatial
504 extent may have also expanded, affecting larger areas over time.

505

506 The third case study focuses on two hazard-related variables, temperature (a proxy for heatwaves) and
507 the SPEI, a proxy of drought, in the Milan area of Italy, both of which are strongly influenced by non-
508 stationarity. The coupling between these variables is well-documented, arising from the interplay
509 between temperature-driven evapotranspiration and the development of dry conditions. At the same
510 time, dry conditions lead to reduced evapotranspiration and greater heat accumulation on land surfaces
511 (e.g., Manning et al., 2019). However, previous studies (e.g., Ribeiro et al., 2020) have often
512 overlooked the impacts of non-stationarity when assessing the joint distribution of their extremes.
513 It is true that the asymptotic justification for the GEV distribution relies on block independence (or
514 weak dependence), and that slowly-varying seasonal phenomena such as droughts and heat waves
515 exhibit temporal correlation structures that may challenge these assumptions. Although SPEI-6
516 represents a slowly-developing process, the GEV distribution has been shown to provide adequate fits
517 for such variables at appropriate aggregation scales. Stagge et al. (2015) demonstrated that GEV
518 outperformed alternative distributions for SPEI across Europe for accumulation periods from 1 to 12
519 months. For the moderate temporal aggregations considered here (monthly temperature, SPEI-6), the
520 GEV provides a practical and empirically supported approximation for extreme value analysis.
521 Alternative approaches such as stochastic generation methods (Parey and Gailhard, 2022) may offer
522 additional rigor for specific applications with stronger temporal dependence. Our analysis revealed
523 pronounced non-stationarity in both variables, with p-values from the Mann-Kendall test close to zero
524 (Figure 4a-b), clearly associated with ongoing climate change and global warming. The Gumbel copula
525 was found to be the most appropriate model for the joint distribution of SPEI and temperature,
526 highlighting their strong coupling during extreme events. Unlike the other two case studies, however,
527 the coupling between these variables lacked a significant trend. This was evidenced by the Mann-
528 Kendall test on the time-varying coupling parameter, which resulted in a p-value of 0.102 (Figure 4c).
529 Given the low significance of the temporal change in the coupling between temperature and SPEI, this
530 case study presented an application where the joint behavior modelled by a Gumbel copula was mostly
531 influenced by non-stationarity of the marginals.

532

533 Final remarks

534

535 In this study, we extended the methodology for non-stationary Extreme Value Analysis (EVA)
536 proposed by Mentaschi et al. (2016) to enable the modeling of joint distributions of extremes that
537 evolve over time. This advancement addresses a critical limitation of univariate EVA, which cannot
538 account for the interdependence among extremes—a crucial aspect in accurately assessing hazards.
539 The framework was tested across a set of case studies involving different hazard-related variables, each
540 exhibiting varying degrees of non-stationarity and interdependence. These examples demonstrate the
541 versatility and generality of the methodology, to accommodate a wide range of environmental variables
542 with distinct characteristics in how extremes are sampled and evolve over the long term. Furthermore,
543 the framework includes techniques to evaluate the significance of modeled changes, enhancing its
544 utility for risk assessment.
545 A remarkable fact is that, in two out of the three case studies, not only do the univariate hazard-related
546 variables exhibit significant temporal changes, but their interdependence also evolves substantially over
547 time. This highlights the importance of adopting a methodology capable of addressing such dynamic
548 relationships, underscoring the relevance of the proposed approach.

549 Additionally, the framework incorporates built-in tools for Monte Carlo simulations, which are
550 instrumental in evaluating goodness-of-fit and estimating uncertainty. Beyond these applications, these
551 simulations can support a more comprehensive risk analysis by generating statistically consistent
552 hazard scenarios, further extending the utility of the methodology.
553 To support future research and applications, we have developed an open-source toolbox, tsEVA 2.0,
554 which accompanies this study. The toolbox, along with the data and examples presented in this paper,
555 is freely available online, offering a practical resource for exploring the joint distributions of non-
556 stationary extremes and fostering advancements in hazard and risk assessment.

557
558

559 Acknowledgements

560 This research has been supported by the European Space Agency (ESA) through the EOatSEE project,
561 contract n° 4000138378/22/I-DT, under the Earth Observation Science for Society block of activities,
562 part of the FutureEO-1 programme. We thank the reviewers for their feedback.

563

564 Code/Data availability

565 All data used in this study, including MATLAB code and input data for each example, are available at
566 <https://github.com/menta78/tsEva> .

567

568 Author contribution

569 M.H. Bahmanpour was responsible for conceptualization, software development, data analysis, and
570 drafting the manuscript. L. Mentaschi contributed to conceptualization, supervision, and manuscript
571 preparation. G. Coppini carried out results investigation, manuscript review, and funding acquisition.
572 The remaining authors contributed to results investigation and manuscript review.

573

574 Competing interests

575 The authors declare that they have no competing interests.

576

577 REFERENCES

578

579 Acero, F. J., Parey, S., Hoang, T. T. H., Dacunha-Castelle, D., García, J. A., & Gallego, M. C. (2017).
580 Non-stationary future return levels for extreme rainfall over Extremadura (southwestern Iberian
581 Peninsula). *Hydrological Sciences Journal*, 62(9), 1394–1411.
582 <https://doi.org/10.1080/02626667.2017.1328559>

583

584 Bevacqua, E., Maraun, D., Hobæk Haff, I., Widmann, M., & Vrac, M. (2017). Multivariate statistical
585 modelling of compound events via pair-copula constructions: analysis of floods in Ravenna (Italy).
586 *Hydrology and Earth System Sciences*, 21(6), 2701–2723. <https://doi.org/10.5194/hess-21-2701-2017>

587

588 Bevacqua, E., Maraun, D., Vousdoukas, M. I., Voukouvalas, E., Vrac, M., Mentaschi, L., & Widmann,
589 M. (2019). Higher probability of compound flooding from precipitation and storm surge in Europe
590 under anthropogenic climate change. *Science Advances*, 5(9), eaaw5531.
591 <https://doi.org/10.1126/sciadv.aaw5531>

592

593 Bender, J., Wahl, T., & Jensen, J. (2014). Multivariate design in the presence of non-stationarity.
594 *Journal of Hydrology*, 514, 123–130. <https://doi.org/10.1016/j.jhydrol.2014.04.017>

595

596 Cannon, A. J. (2010). A flexible nonlinear modelling framework for nonstationary generalized extreme
597 value analysis in hydroclimatology. *Hydrological Processes*, 24(6), 673–685.
598 <https://doi.org/10.1002/hyp.7506>
599

600 Cheng, L., AghaKouchak, A., Gilleland, E., & Katz, R. W. (2014). Non-stationary extreme value
601 analysis in a changing climate. *Climatic Change*, 127(2), 353–369. <https://doi.org/10.1007/s10584-014-1254-5>
602

603

604 Coles, S. (2001). *An introduction to statistical modeling of extreme values*. Springer.

605

606 Dosio, A., Mentaschi, L., Fischer, E. M., & Wyser, K. (2018). Extreme heat waves under 1.5 °C and
607 2 °C global warming. *Environmental Research Letters*, 13(5), 054006. <https://doi.org/10.1088/1748-9326/aab827>
608

609

610 Dottori, F., Mentaschi, L., Bianchi, A., Alfieri, L., & Feyen, L. (2023). Cost-effective adaptation
611 strategies to rising river flood risk in Europe. *Nature Climate Change*, 13(2), 196–202.
612 <https://doi.org/10.1038/s41558-022-01540-0>
613

614 Genest, C., Rémillard, B., & Beaudoin, D. (2009). Goodness-of-fit tests for copulas: A review and a
615 power study. *Insurance: Mathematics and Economics*, 44(2), 199–213.
616 <https://doi.org/10.1016/j.insmatheco.2007.10.005>
617

618 Hamed, K. H. (2008). Trend detection in hydrologic data: The Mann–Kendall trend test under the
619 scaling hypothesis. *Journal of Hydrology*, 349(3), 350–363.
620 <https://doi.org/10.1016/j.jhydrol.2007.11.009>
621

622 Hamed, K. H., & Rao, A. R. (1998). A modified Mann-Kendall trend test for autocorrelated data.
623 *Journal of Hydrology*, 204(1), 182–196. [https://doi.org/10.1016/S0022-1694\(97\)00125-X](https://doi.org/10.1016/S0022-1694(97)00125-X)
624

625 Jane, R., Dalla Valle, L., Simmonds, D., & Raby, A. (2016). A copula-based approach for the
626 estimation of wave height records through spatial correlation. *Coastal Engineering*, 117, 1–18.
627 <https://doi.org/10.1016/j.coastaleng.2016.06.008>
628

629 Jiang, C., Xiong, L., Xu, C.-Y., & Guo, S. (2015). Bivariate frequency analysis of nonstationary low-
630 flow series based on the time-varying copula. *Hydrological Processes*, 29(6), 1521–1534.
631 <https://doi.org/10.1002/hyp.10288>
632

633 Jiang, S., Bevacqua, E., & Zscheischler, J. (2022). River flooding mechanisms and their changes in
634 Europe revealed by explainable machine learning. *Hydrology and Earth System Sciences*, 26(24),
635 6339–6359. <https://doi.org/10.5194/hess-26-6339-2022>
636

637 Joe, H. (1997). *Multivariate Models and Multivariate Dependence Concepts* (1st ed.). Chapman and
638 Hall/CRC. <https://doi.org/10.1201/9780367803896>
639

640 Li, H., Wang, D., Singh, V. P., Wang, Y., Wu, J., Wu, J., Liu, J., Zou, Y., He, R., & Zhang, J. (2019).
641 Non-stationary frequency analysis of annual extreme rainfall volume and intensity using Archimedean

642 copulas: A case study in eastern China. *Journal of Hydrology*, 571, 114–131.
643 <https://doi.org/10.1016/j.jhydrol.2019.01.054>
644

645 Manning, C., Widmann, M., Bevacqua, E., van Loon, A. F., Maraun, D., & Vrac, M. (2019). Increased
646 probability of compound long-duration dry and hot events in Europe during summer (1950–2013).
647 *Environmental Research Letters*, 14(9), 094006. <https://doi.org/10.1088/1748-9326/ab23bf>
648

649 Mentaschi, L., Vousdoukas, M. I., Voukouvalas, E., Sartini, L., Feyen, L., Besio, G., & Alfieri, L.
650 (2016). The transformed-stationary approach: a generic and simplified methodology for non-stationary
651 extreme value analysis. *Hydrology and Earth System Sciences*, 20(9), 3527–3547.
652 <https://doi.org/10.5194/hess-20-3527-2016>
653

654 Mentaschi, L., Vousdoukas, M. I., Voukouvalas, E., Dosio, A., & Feyen, L. (2017). Global changes of
655 extreme coastal wave energy fluxes triggered by intensified teleconnection patterns. *Geophysical*
656 *Research Letters*, 44(5), 2416–2426. <https://doi.org/10.1002/2016GL072488>
657

658 Mentaschi, L., Vousdoukas, M. I., García-Sánchez, G., Fernández-Montblanc, T., Roland, A.,
659 Voukouvalas, E., Federico, I., Abdolali, A., Zhang, Y. J., & Feyen, L. (2023). A global unstructured,
660 coupled, high-resolution hindcast of waves and storm surge. *Frontiers in Marine Science*, 10.
661 <https://doi.org/10.3389/fmars.2023.1233679>
662

663 Naumann, G., Cammalleri, C., Mentaschi, L., & Feyen, L. (2021). Increased economic drought impacts
664 in Europe with anthropogenic warming. *Nature Climate Change*, 11(6), 485–491.
665 <https://doi.org/10.1038/s41558-021-01044-3>
666

667 Nelsen, R. B. (2006). *An introduction to copulas*. Springer. <https://doi.org/10.1007/0-387-28678-0>
668

669 Parey, S., Hoang, T. T. H., & Dacunha-Castelle, D. (2010). Different ways to compute temperature
670 return levels in the climate change context. *Environmetrics*, 21(7–8), 698–718.
671 <https://doi.org/10.1002/env.1060>
672

673 Parey, S., Hoang, T. T. H., & Dacunha-Castelle, D. (2013). The importance of mean and variance in
674 predicting changes in temperature extremes. *Journal of Geophysical Research: Atmospheres*, 118(15),
675 8285–8296. <https://doi.org/10.1002/jgrd.50629>
676

677 Parey, S., Hoang, T. T. H., & Dacunha-Castelle, D. (2019). Future high-temperature extremes and
678 stationarity. *Natural Hazards*, 98(3), 1115–1134. <https://doi.org/10.1007/s11069-018-3499-1>
679

680 Parey, S., & Gailhard, J. (2022). Extreme Low Flow Estimation under Climate Change. *Atmosphere*,
681 13(2). <https://doi.org/10.3390/atmos13020164>
682

683 Ribeiro, A. F. S., Russo, A., Gouveia, C. M., & Pires, C. A. L. (2020). Drought-related hot summers: A
684 joint probability analysis in the Iberian Peninsula. *Weather and Climate Extremes*, 30, 100279.
685 <https://doi.org/10.1016/j.wace.2020.100279>
686

687 Salvadori, G., Durante, F., de Michele, C., Bernardi, M., & Petrella, L. (2016). A multivariate copula-
688 based framework for dealing with hazard scenarios and failure probabilities. *Water Resources*
689 *Research*, 52(5), 3701–3721. <https://doi.org/10.1002/2015WR017225>

690
691 Sarhadi, A., Burn, D. H., Concepción Ausín, M., & Wiper, M. P. (2016). Time-varying nonstationary
692 multivariate risk analysis using a dynamic Bayesian copula. *Water Resources Research*, 52(3), 2327–
693 2349. <https://doi.org/10.1002/2015WR018525>
694
695 Seinaldi, F. (2015). Dismissing return periods! *Stochastic Environmental Research and Risk*
696 *Assessment*, 29(4), 1179–1189. <https://doi.org/10.1007/s00477-014-0916-1>
697
698 Shooter, R., Ross, E., Ribal, A., Young, I. R., & Jonathan, P. (2021). Spatial dependence of extreme
699 seas in the North East Atlantic from satellite altimeter measurements. *Environmetrics*, 32(4), e2674.
700 <https://doi.org/10.1002/env.2674>
701
702 Sklar, A. (1959). Fonctions de répartition à n dimensions et leurs marges. *Publications de l'Institut de*
703 *Statistique de l'Université de Paris*, 8, 229–231.
704
705 Sklar, A. (1973). Random variables, joint distribution functions, and copulas. *Kybernetika*, 9(6), 449–
706 460.
707
708 Stagge, J. H., Tallaksen, L. M., Gudmundsson, L., van Loon, A. F., & Stahl, K. (2015). Candidate
709 Distributions for Climatological Drought Indices (SPI and SPEI). *International Journal of Climatology*,
710 35(13), 4027–4040. <https://doi.org/10.1002/joc.4267>
711
712 Tilloy, A., Malamud, B. D., Winter, H., & Joly-Laugel, A. (2020). Evaluating the efficacy of bivariate
713 extreme modelling approaches for multi-hazard scenarios. *Natural Hazards and Earth System Sciences*,
714 20(8), 2091–2117. <https://doi.org/10.5194/nhess-20-2091-2020>
715
716 Tilloy, A., Paprotny, D., Grimaldi, S., Gomes, G., Bianchi, A., Lange, S., Beck, H., Mazzetti, C., &
717 Feyen, L. (2025). HERA: a high-resolution pan-European hydrological reanalysis (1951–2020). *Earth*
718 *System Science Data*, 17(1), 293–316. <https://doi.org/10.5194/essd-17-293-2025>
719
720 Wahl, T., Jain, S., Bender, J., Meyers, S. D., & Luther, M. E. (2015). Increasing risk of compound
721 flooding from storm surge and rainfall for major US cities. *Nature Climate Change*, 5(12), 1093–1097.
722 <https://doi.org/10.1038/nclimate2736>
723
724 Wang, R., Liu, J., & Wang, J. (2024). The extremal spatial dependence of significant wave height in
725 the South China sea. *Ocean Engineering*, 295, 116888. <https://doi.org/10.1016/j.oceaneng.2024.116888>
726
727 Vousdoukas, M. I., Mentaschi, L., Voukouvalas, E., Verlaan, M., Jevrejeva, S., Jackson, L. P., &
728 Feyen, L. (2018). Global probabilistic projections of extreme sea levels show intensification of coastal
729 flood hazard. *Nature Communications*, 9(1), 2360. <https://doi.org/10.1038/s41467-018-04692-w>
730
731 Vousdoukas, M. I., Mentaschi, L., Hinkel, J., Ward, P. J., Mongelli, I., Ciscar, J.-C., & Feyen, L.
732 (2020). Economic motivation for raising coastal flood defenses in Europe. *Nature Communications*,
733 11(1), 2119. <https://doi.org/10.1038/s41467-020-15665-3>
734
735 Yue, S., & Wang, C. (2004). The Mann-Kendall Test Modified by Effective Sample Size to Detect
736 Trend in Serially Correlated Hydrological Series. *Water Resources Management*, 18(3), 201–218.
737 <https://doi.org/10.1023/B:WARM.0000043140.61082.60>

738

739 Zscheischler, J., Martius, O., Westra, S., Bevacqua, E., Raymond, C., Horton, R. M., van den Hurk, B.,
740 AghaKouchak, A., Jézéquel, A., Mahecha, M. D., Maraun, D., Ramos, A. M., Ridder, N. N., Thiery,
741 W., & Vignotto, E. (2020). A typology of compound weather and climate events. *Nature Reviews*
742 *Earth & Environment*, 1(7), 333–347. <https://doi.org/10.1038/s43017-020-0060-z>

743

744 Zscheischler, J., Westra, S., van den Hurk, B. J. J. M., Seneviratne, S. I., Ward, P. J., Pitman, A.,
745 AghaKouchak, A., Bresch, D. N., Leonard, M., Wahl, T., & Zhang, X. (2018). Future climate risk from
746 compound events. *Nature Climate Change*, 8(6), 469–477. <https://doi.org/10.1038/s41558-018-0156-3>

747

748 Zheng, F., Westra, S., Leonard, M., & Sisson, S. A. (2014). Modeling dependence between extreme
749 rainfall and storm surge to estimate coastal flooding risk. *Water Resources Research*, 50(3), 2050–
750 2071. <https://doi.org/10.1002/2013WR014616>

751

752 Zhang, X. (2023). A dataset of monthly SPI and SPEI derived from ERA5 over 1959–2022 [Data set].
753 Figshare. <https://doi.org/10.6084/m9.figshare.24485389.v1>

754